

Ordered Vacancies and Their Chemistry in Metal–Organic Frameworks

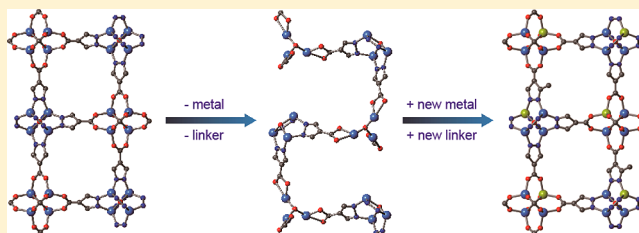
Binbin Tu,[†] Qingqing Pang,[†] Doufeng Wu,[†] Yuna Song,[‡] Linhong Weng,[†] and Qiaowei Li^{*†}

[†]Department of Chemistry, Fudan University, 220 Handan Road, Shanghai 200433, China

[‡]School of Chemistry, Beijing Institute of Technology, 5 Zhongguancun South Street, Beijing 100081, China

S Supporting Information

ABSTRACT: Vacancies are common in solid materials, but it remains a challenge to introduce them at specific locations with controlled distributions. Here we report the creation of ordered metal vacancies and linker vacancies in a cubic metal–organic framework (MOF) based on Zn(II) and pyrazole-carboxylic acid by removing a quarter of the metal ions and half of the linkers. The MOF with ordered vacancies shows increased pore size, thus allowing large dye molecules to fit in the pores. Furthermore, by filling the vacancies with new metals and new linkers, eight new single-crystalline MOFs with multicomponents in absolute order are introduced. The capability of performing stepwise elimination and addition reactions systematically in extended solids without destroying the structural integrity has generated complex MOF structures which otherwise cannot be made.



INTRODUCTION

Vacancies in crystalline solids are well-known and have been extensively studied for the impact they make on the electrical, optical, magnetic, and catalytic properties of materials.¹ Generally, these vacancies are missing ions or atoms in an ordered lattice in which they are often found to be randomly distributed, and in few cases, they are ordered.^{2–5} They do, however, constitute a minority yet an important part of the overall structure of the material. Although such vacancies are easily found in solids, it remains a challenge to introduce them in a deliberate manner at specific locations with precise control over their distributions. This is attributable to the fact that harsh conditions (e.g., high temperature,^{6,7} addition of mineralizers^{8,9}) are typically required for generating vacancies in solids. In this report, we show how ordered vacancies can be successfully generated in metal–organic frameworks (MOFs),^{10–14} and how the resulting framework can be functionalized by carrying out chemistry on those created vacancies.

Specifically, we use as an exemplar a three-dimensional porous MOF (**1**, Zn₄O(PyC)₃, PyC = 4-pyrazolecarboxylate) constructed from Zn₄O(COO)₆ and Zn₄ON₁₂ units linked by PyC. We demonstrate the creation of vacancies by removal of half of the linkers and a quarter of the metal ions from crystals of **1** to make **2** (Zn₃□₁(OH)(PyC)_{1.5}□_{1.5}(OH)(H₂O)_{3.5}·(PyC)_{0.5}, □: vacancy) with full retention of single crystallinity and the original unit cell dimensions (Figure 1a). Accordingly, the structure of **2** shows the systematically ordered appearance of vacant sites originally occupied by the linkers and metal ions and exhibits a corresponding increase in the pore size. We further show that the metal vacancies can be filled with new metal ions (Li⁺, Co²⁺, Cd²⁺, and La³⁺) and the linker vacancies

with new functionalized linkers (CH₃–PyC and NH₂–PyC)—reactions which can be carried out separately or in a combined step. While defects have been obtained by linker fragmentation during crystal growth^{15–18} and random vacancies have been created by acid etching in MOFs,¹⁹ the presented cycle of making a MOF without vacancies, creating ordered vacancies in that MOF, and filling such vacancies with new modules is fundamentally important because it generates more complex MOFs which otherwise cannot be made.

RESULTS AND DISCUSSION

Here, we outline the synthesis and characterization of all materials produced without and with vacancies and the associated chemistry to fill those vacancies.

Creating Ordered Metal and Linker Vacancies in MOFs by Elimination Reactions. Solvothermal reaction of Zn(NO₃)₂·6H₂O with H₂PyC in *N,N*-diethylformamide (DEF) at 100 °C for 48 h affords single crystals of Zn₄O(PyC)₃, noted as **1**. Single-crystal X-ray diffraction reveals that structure **1** is cubic, where two types of secondary building units (SBUs)²⁰ are connected by the PyC (Figure 2a and Table S1 in the Supporting Information). Specifically, N in pyrazolate and O in carboxylate coordinate to Zn(II), and they self-organize into Zn₄ON₁₂ and Zn₄O(COO)₆, acting as two sets of octahedral SBUs (Figure 1b) that are arranged alternatively along the network. This structure crystallizes in chiral *F*23,²¹ with *a* = 20.09 Å. The almost identical coordination features of the pyrazolate and the carboxylate make structure **1** analogous to MOF-5.²²

Received: June 24, 2014

Published: September 17, 2014

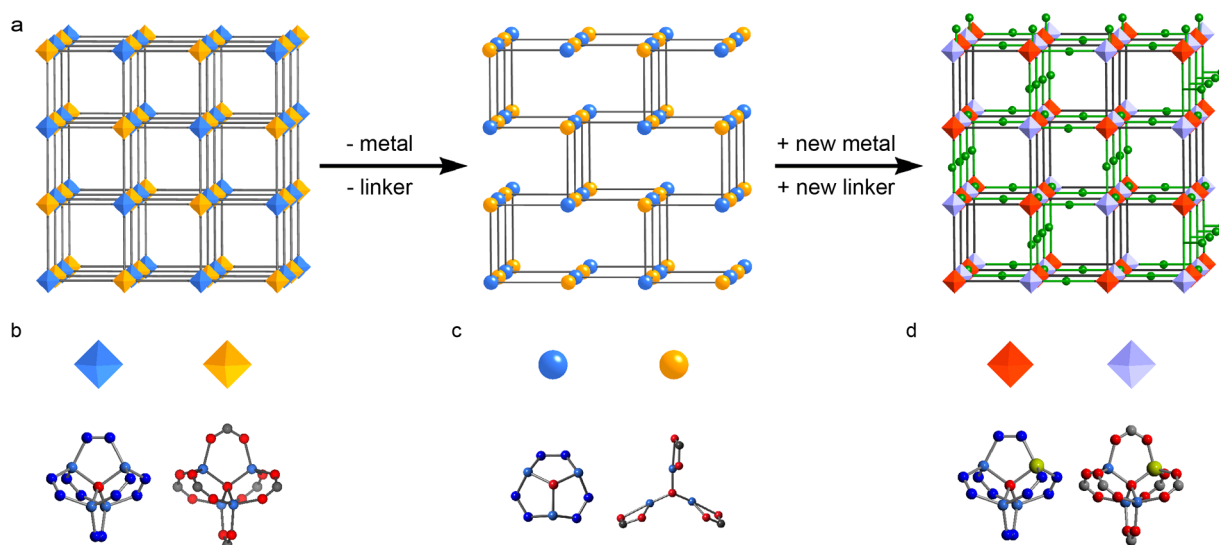


Figure 1. Schematic illustration of a framework undergoing metal and linker elimination reactions and new metal and new linker addition reactions in single-crystal form. A cubic structure (a, left) containing two types of octahedral secondary building units (SBUs) (b) transforms itself into a new structure (a, middle) with two types of triangular SBUs (c) by creating ordered metal and linker vacancies. This structure could process a second-step transformation by filling the vacancies with new metals and new linkers (a, right), resulting in a framework with two types of heterometallic octahedral SBUs (d) and two types of linkers arranged in order. Color scheme in b, c, and d: original metal, light blue; new metal, green; C, gray; N, dark blue; O, red.

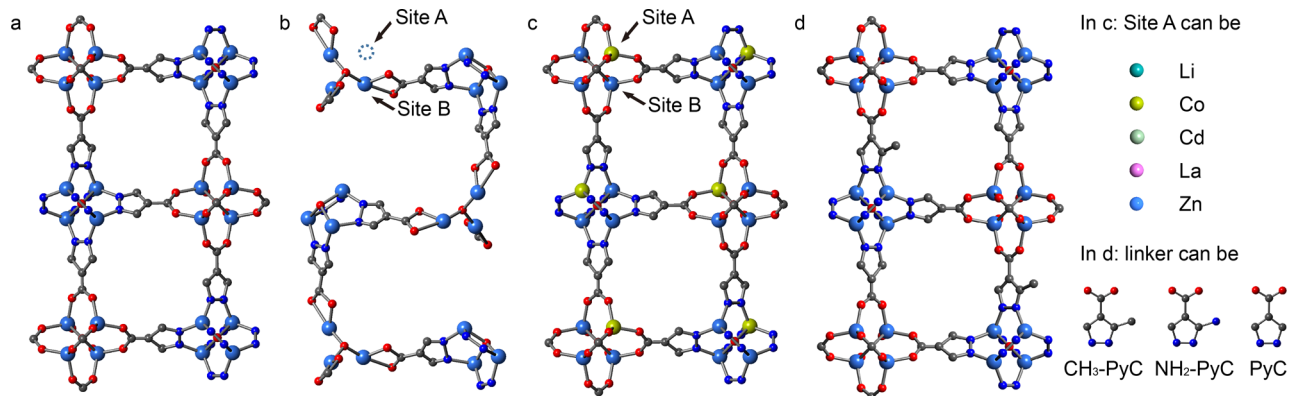


Figure 2. Single-crystal structures of the MOFs without vacancies, with vacancies, and with new modules filled in the vacancies. Superimposition of the structures 1 (a), 2 (b), 3-Co (c), and 4-CH₃ (d) reveals the ordered sites where the elimination and addition of metals and linkers take place. Zn, light blue; C, gray; N, dark blue; O, red.

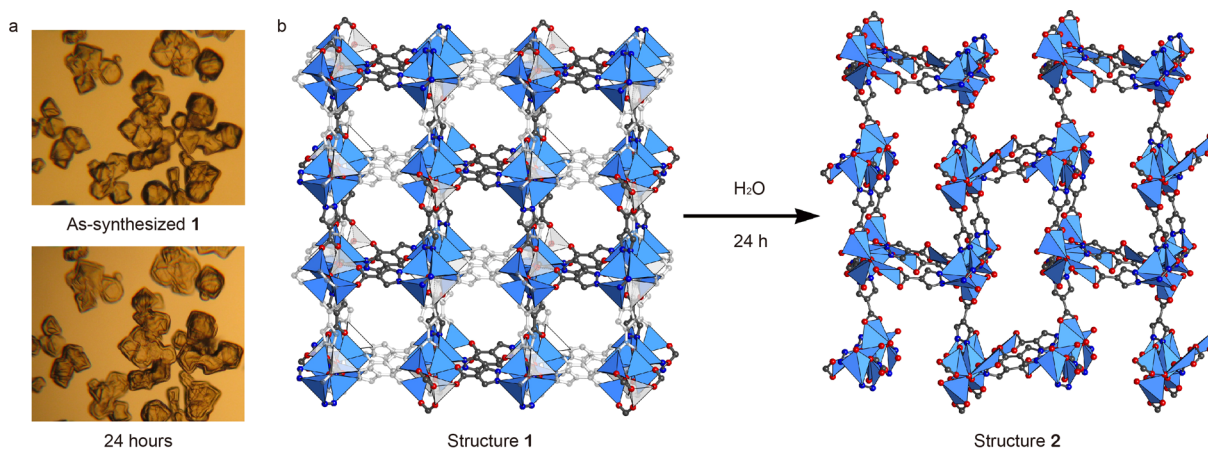


Figure 3. (a) Still images of crystals taken at 0 and 24 h after structure 1 was immersed in water suggest a single-crystal to single-crystal transformation. (b) A quarter of the metal ions and half of the linkers (shown in translucent form) of structure 1 are removed to generate structure 2 with ordered metal vacancies and linker vacancies. Zn, light blue polyhedra; C, gray spheres; N, dark blue spheres; O, red spheres.

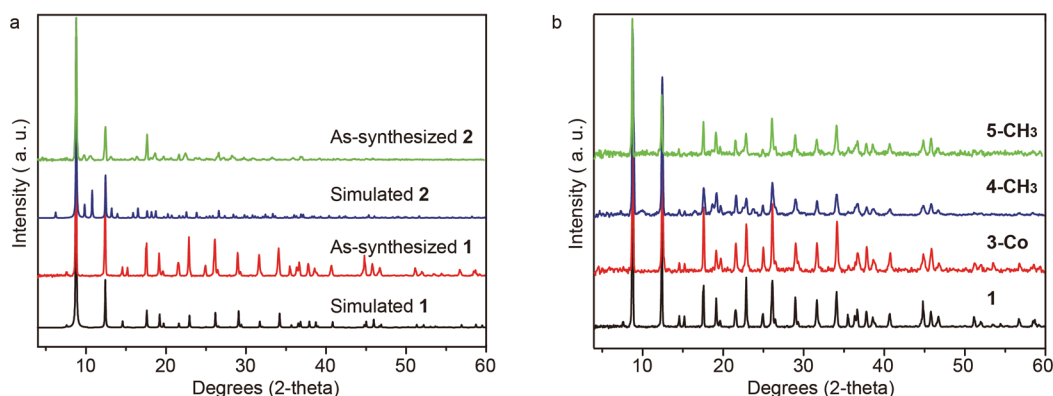
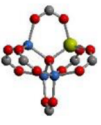
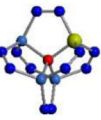


Figure 4. Powder X-ray diffraction (XRD) patterns of as-synthesized **1** and **2** (a) and those of as-synthesized **1**, **3-Co**, **4-CH₃**, and **5-CH₃** (b), along with their corresponding simulated patterns based on the single-crystal X-ray data.

Table 1. Zn:M Ratio and Selected Bond Lengths in the SBUs for Structures **1** and **3-M^a**

MOFs		1	3-Li	3-Co	3-Cd	3-La
Zn:M ratio in each SBU		—	3.84:0.16	3.05:0.95	3.64:0.36	3.86:0.14
New metal occupancy in Site A		—	16%	95%	36%	14%
	Zn-μ ₄ -O bond length	1.9605(14)	1.928(2)	1.964(4)	1.985(4)	1.971(3)
	Zn/M-μ ₄ -O bond length	—	2.060(7)	1.946(10)	1.825(10)	1.866(8)
	Zn-μ ₄ -O bond length	1.9499(14)	1.966(2)	2.019(4)	1.951(3)	1.942(2)
	Zn/M-μ ₄ -O bond length	—	1.954(6)	1.811(9)	1.999(7)	2.021(7)

^aThe distances between Zn or Zn/M (shown in green) and μ₄-O (O in the center of SBUs) are listed. Zn:M ratios are determined by ICP-AES, and the bond lengths with estimated standard deviations (esd's) are determined by the single-crystal X-ray diffraction. The ratios are reported as the sum of Zn and M being four, which corresponds to four metal sites in each SBU.

Upon immersion of crystals of **1** in water at room temperature, we observe the transformation of **1** to **2**, Zn₃(OH)(PyC)_{1.5}(OH)(H₂O)_{3.5}(PyC)_{0.5}, in 24 h.

The formula of structure **2** is determined by the single-crystal X-ray diffraction along with elemental analysis, in which the additional PyC serve as counteranions to the cationic framework (see the Supporting Information). The octahedral morphology of the crystals remains intact during the transformation, as confirmed by the images taken throughout the process (Figure 3a and Figure S5 in the Supporting Information). **2** remains single-crystal quality, which allows us to examine its structure by single-crystal X-ray diffraction. Interestingly, structure **2** (Figure 2b) contains two kinds of triangular SBUs, Zn₃(OH)N₆ and Zn₃(OH)(COO)₃ (Figure 1c), which is different from the octahedral Zn₃(OH)N₆(COO)₃ SBU as in the case of MOF-324,²³ and applying both of them as building blocks in one single structure is unprecedented. In structure **2**, each SBU is connected to three organic linkers, resulting in a three-dimensional MOF in srs topology.²⁴

The single-crystal to single-crystal transformation (Figure 3b) from **1** to **2** is achieved by (i) taking out one Zn atom in each SBU and (ii) the excision of half of the linkers from the framework completely, with the coordination around the metals further saturated by incoming H₂O molecules. The three

remaining organic linkers around each SBU are still perpendicular to each other, generating a network with rectangular channels. The cell dimensions of **2** ($a = 20.09$ Å) are identical to that of **1** with the space group reduced to slightly lower symmetry ($P2_13$), accounting for the formation of metal vacancies and linker vacancies. We confirm the homogeneity of the bulk materials **1** and **2** by their powder X-ray diffraction (XRD) where their diffraction patterns match those simulated from the single-crystal X-ray data (Figure 4a).

The positions of the missing metals and linkers represent the vacancies, and their order is confirmed by the crystallographic regularity of **2**. We observe that when the immersion of **1** in water is done for a shorter time the elimination reaction is incomplete and probably with a random distribution of vacancies in the structure, while a longer time for this reaction results in the appearance of a second phase in the crystals, which is a two-dimensional MOF structure (Zn(PyC)(H₂O), Figure S1, Supporting Information). Thus, it is worthy to note that the regularity of vacancies in **2**, although not expected, is observed because of a right time window for the right number, which happens to be the maximum number, of vacancies to form without architectural collapse of the structure. In a way, the conversion of the **1** to **2** process is akin to the removal of nonload-bearing walls of a building. Importantly, only subtle

rearrangement of the remaining linkers is involved during the symmetry-guided creation of the vacancies. The systematic excision is driven by (i) the coordination of the metal ions with the H₂O molecules and (ii) the favorable entropy by releasing free metal ions and linkers, and this single-crystal to single-crystal process is facilitated by the reversible metal–linker coordination.

Interconnected channels in **1** and **2** facilitate the release of metal ions and linkers and the subsequent diffusion out of the crystal. Following the transformation, addition of aqueous Na₂S solution to the supernatant results in a substantial amount of white ZnS precipitate, confirming the presence of Zn²⁺ freed from the framework. Solution-state ¹H NMR of the white powder obtained by evaporating the supernatant also demonstrates the presence of pyrazolecarboxylate (Figure S15, Supporting Information). The porous nature of these MOF structures allows the efficient transportation of ions in the pores without blocking them.

Filling Ordered Metal Vacancies with New Metal Ions.

A second-step single-crystal to single-crystal transformation is performed by the immersion of structure **2** in DEF solutions of different metal ions (Li⁺, Co²⁺, Cd²⁺, or La³⁺) at 100 °C for 3 days. The dissolution–recrystallization mechanism was ruled out by monitoring the shape and the amount of crystals during the reactions closely (Figure S6, Supporting Information). The obtained structures (3-**M**, Zn_{4-x}M_xO(PyC)₃, M = Li, Co, Cd, and La) are still in single-crystal form, which makes single-crystal X-ray analysis possible (Table S2, Supporting Information).

The 3-**M** series (Figures 2c and 4b) is isostructural with structure **1**. However, instead of the *F*23 space group for structure **1**, the 3-**M** series possesses *P*₂₁₃ space group. This indicates that in each SBU one metal site (Site A in Figure 2c) is not identical with the other three sites (Site B), suggesting the possible formation of heterometallic SBUs. A closer investigation of the bond lengths (Table 1) between the metals and the μ₄-O in the center of the SBUs, which belongs to the most rigid part of the structure in spite of the disordered nature of the framework, reveals that the bond lengths involving Site A are more deviated from those of the typical Zn–O in MOFs. What is more, the estimated standard deviations (esd's) of bond lengths involving Site A are significantly higher than those involving Site B. A superimposition of structure **2** and 3-**M** reasonably points out that Site A was the vacancy sites, and now the metals fill them during this second-step transformation. On the other hand, Site B which was fully occupied by Zn(II), remains intact, thus showing lower esd's with typical Zn–O bond lengths.

These heterometallic MOFs show different M/Zn ratios in the SBUs, due to the various metal–linker coordinations. For example, Li(I), Cd(II), and La(III), with different coordination numbers and different M–O and M–N bond lengths, show relatively low occupancies in Site A from 14% to 36%, as determined by the ICP-AES (Table 1 and Table S4 in the Supporting Information). Since new metals introduce distortions to the framework, 3-**M** with low occupancy of new metals is thermodynamically favored. A majority of the vacancies were backed up by Zn(II), which is believed to have been provided by the sacrifice of some frameworks. The sacrifice also feeds linkers needed to recover the cubic network, in addition to the free PyC which were in the pores as charge-compensating ions for the cationic framework of **2**. The coordination of the newly installed metals is further saturated

by solvents, with the charge balanced by compensating ions. Powder XRD patterns of the crystals after the transformation confirm that no new solids are formed, as evidenced by all the peaks corresponding to the simulated pattern of 3-**M** (Figure S2, Supporting Information). This method demonstrates the successful systematic filling of various metal ions with different coordination numbers, radius, and valences into ordered vacancies in the crystals.

In the vacancy filling with Co²⁺, we observe that its ratio with Zn²⁺ is 0.95:3.05, which suggests that Site A is filled with Co(II) dominantly, as determined by the ICP-AES. Considering the similar ionic radius and coordination mode, Co²⁺ could occupy the ordered vacancies without introducing serious structural distortion. With much less Zn²⁺ available in the solution, Co²⁺ occupies these vacancy sites. This kinetics-driven process leads to single crystals composed of SBUs containing exactly three zinc ions in Site B and one cobalt ion in Site A in order (Figure 1d). Our studies show that using higher concentration of Co²⁺ does not lead to more Co(II) in the framework. The unique structural features of **2** make it act as a basis to introduce complexities in crystalline solids by precrafting numerous vacancy sites. The absolute ordered distribution of two similar metals at the atomic level with a well-defined chemical environment could not be achieved by other postsynthetic methods^{25–47} reported for MOFs.

Filling Ordered Linker Vacancies with New Linkers.

The ordered linker vacancies in structure **2** also allow new linkers with different functionalities to coordinate with metal ions and to regenerate cubic networks with multifunctionalities. Specifically, crystals of **2** were immersed in a DEF solution of pyrazolecarboxylic acid with –CH₃ or –NH₂ functionality at 100 °C for 3 days, resulting in new crystals we termed 4-**L** (Zn₄O(PyC)_{3-y}L_y; 4-**CH**₃ for L = CH₃–PyC, 4-**NH**₂ for L = NH₂–PyC). Single-crystal X-ray diffraction (Table S3, Supporting Information) of 4-**L** shows that these structures crystallize in *F*23,²¹ where the PyC with and without functionalities and two types of SBUs assemble into cubic structures isostructural to **1** (Figure 2d and 4b and Figure S3 in the Supporting Information).

The ratios between different linkers in **4** are determined by solution-state ¹H NMR of the deuterated HCl-digested MOF samples. In 4-**CH**₃, CH₃–PyC accounts for 42% of the total linkers in the crystals (Figure S16, Supporting Information). The value is lower than the ideal 50% because PyC exist in the pores as the compensating ions in **2**, and they also participate in the linker vacancy filling. For 4-**NH**₂, the percentage of NH₂–PyC is 29% when the same linker concentration was used as in 4-**CH**₃ (Figure S17, Supporting Information). This trend of lower ratio has been observed in the previous –NH₂-containing MTV–MOFs made by linker mixing strategy.⁴⁸

While it is impossible to locate the positions of –CH₃ or –NH₂ accurately even at lower space group (for example *P*₂₁₃) due to positional disorder, it is tempting to propose logical arrangement of the two kinds of linkers in the crystals. Upon heating in DEF, the substitutions of water molecules around the linker vacancies with the new linkers are thermodynamically more favorable than the displacement of the pre-existing PyC. What is more, the percentage of CH₃–PyC does not increase even when higher concentration (up to five times the original concentration) is employed for 4-**CH**₃, suggesting CH₃–PyC go to the predesigned linker vacancies rather than simply perform linker exchange with PyC. Compared to its analogue obtained by solvent-assisted linker exchange (immersion of **1**

into DEF solution of $\text{CH}_3\text{-H}_2\text{PyC}$ with heating), structure **4-CH₃** shows new linkers at very specific sites deliberately controlled by the ordered vacancies. Moreover, MOFs containing $\text{NH}_2\text{-PyC}$ could not be obtained either by the linker exchange method or by one-pot reaction under various MOF synthesis conditions performed, demonstrating the capability of making new structures that could not be made in other ways.

One-Step Filling of Both Metal and Linker Vacancies with New Metals and New Linkers. With the capability of accepting both metal ions and organic linkers into the framework by occupying the prearranged vacancies, structure **2** is employed to construct MOFs containing two kinds of metals and two kinds of linkers in one pot. $\text{Zn}_{4-x}\text{Co}_x\text{O}(\text{PyC})_{3-y}\text{L}_y$ (**5-CH₃** for $\text{L} = \text{CH}_3\text{-PyC}$, $x = 1.01$, $y = 1.44$; **5-NH₂** for $\text{L} = \text{NH}_2\text{-PyC}$, $x = 0.78$, $y = 0.66$) were obtained by immersing single crystals of **2** in a DEF solution of both the functionalized linker and cobalt nitrate (Figure 5). The single-

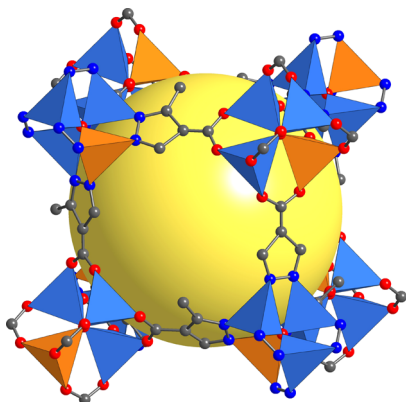


Figure 5. Single-crystal structure of **5-CH₃** with one cube composed of $\text{Zn}_3\text{CoON}_{12}$ and $\text{Zn}_3\text{CoO}(\text{COO})_6$ SBUs, PyC, and $\text{CH}_3\text{-PyC}$ in absolute order shown. The yellow sphere of diameter 10.8 Å illustrates the empty space inside the cube. Zn, light blue; Co, orange; C, gray; N, dark blue; O, red.

crystal structural analysis (Table S3, Supporting Information) of **5-CH₃** and **5-NH₂** reveals their isoreticular network with structure **1** (Figure 4b and Figure S4 in the Supporting Information), with the ratio of two kinds of metals and two kinds of linkers determined by ICP-AES (Table S4, Supporting Information) and ^1H NMR spectroscopy (Figures S18 and S19, Supporting Information), respectively. During the construction of **5-CH₃**, the additions of Co(II) and $\text{CH}_3\text{-PyC}$ to the framework does not interfere with each other, as supported by the ratio of metals and linkers in **5-CH₃** ($\text{Zn}:\text{Co} = 2.99:1.01$, $\text{PyC}:\text{CH}_3\text{-PyC} = 1:56:1.44$) being similar to those in **3-Co** and **4-CH₃**. What is more, these ratios are determined by the ratios between preoccupied sites and vacancy sites for metals and linkers in **2** (3:1 and 1.5:1.5, respectively).

With two kinds of metal ions and two kinds of linkers in the system, it is possible to obtain four different MOFs based on one single metal and one linker by routine solvothermal reactions. It is also possible to construct multifunctional MOFs with mixed metals and/or linkers,^{16,17,48–58} in which the composition and the order are difficult to control when the connectivities are similar to each other. Despite the high similarity between Zn(II) and Co(II) and between PyC and $\text{CH}_3\text{-PyC}$, we are able to place them in exact order within the whole crystal. After elimination and addition reactions involving

both metals and linkers as parts of the skeleton, **5-CH₃** represents networks with two types of heterometallic inorganic building units and two kinds of organic linkers in absolute order (Figure 5). Equivalent to functionalizing small molecules step by step, the system here demonstrates an example of performing stepwise reactions in crystalline solids, and what is more, without destroying the architectural integrity.⁵⁹

Porosity of MOFs without and with Vacancies. It is noteworthy that $\text{Zn}_4\text{O}(\text{dmcapz})_3$ ($\text{dmcapz} = 3,5\text{-dimethyl-4-carboxypyrazolato}$), a structure determined by powder XRD, shares an analogous framework with structure **1** and was first reported by J. A. R. Navarro.⁶⁰ With a slenderer linker, structure **1** has relatively larger pore size. It features large and small pores (10.8 and 7.6 Å in diameter, respectively), with the pore aperture of 4.5 Å in diameter. The porosity of **1** is assessed by performing N_2 adsorption isotherms at 77 K subsequent to sample activation (Figure 6a). The isotherm exhibits a Type-I behavior, which is typical of microporous MOFs, with a Brunauer–Emmett–Teller (BET) surface area of $1249 \text{ m}^2 \text{ g}^{-1}$. After creating vacancies by the removal of the metal ions and the linkers, structure **2** constitutes rectangular channels with the diagonal of the aperture ~ 13.0 Å, showing a BET surface area of $1144 \text{ m}^2 \text{ g}^{-1}$. Hysteresis can be observed in the N_2 isotherm of structure **2**, which corresponds to the defects,^{61,62} such as mesopore formation as a result of fragmentary framework collapse during the transformation. The increase of the adsorbed amounts of N_2 (387 and 546 mg g^{-1} for **1** and **2** at P_0 , respectively) is observed, along with the crystal density reduction from 1.00 to 0.74 g cm^{-3} during the transformation.

Low-pressure N_2 adsorption isotherms of structures **3-M**, **4-L**, and **5-L** (Figures S7–S9, Supporting Information) reveal that the multimetal and/or multilinker systems retain their original porosity after two steps of reactions on the single crystals, and their surface area values are listed in the Supporting Information Table S5. The hysteresis in the isotherms of these MOFs is attributed to the mesopores formed by the sacrifice of the framework to provide metal ions and/or linkers needed. For **3-Co** and **4-CH₃**, the hysteresis is more obvious because higher occupancies of new metals and new linkers introduce more defects to the crystals. Micropore size distribution analyses of all MOFs show narrow micropore distributions (Figures S10–S14, see the Supporting Information). Thermogravimetric analysis (Figures S22–S25, Supporting Information) indicates these MOFs exhibit similar thermal stability with the main weight loss starting at around 300 °C.

The pore size and shape transformation by creating vacancies is also assessed by the inclusion of acridine red molecules into the pores of the crystals. Acridine red, with a size of $14.2 \times 8.3 \times 3.7$ Å³, could diffuse into the pores of structure **2** with rectangular openings. Visual examination reveals that the crystals of **2** turn orange upon immersion in the ethanol solution of acridine red. The acridine red amount in the pores was determined by the ^1H NMR spectroscopy after the crystals were washed, dried, and then digested in deuterated HCl. In structure **2**, the ratio of PyC to acridine red is 10.5:1 (Figure S20, Supporting Information), which corresponds to about one acridine red molecule in each unit cell. Remarkably, the acridine red in structure **2** maintains the original high crystallinity of the parent framework, as confirmed by their coincident powder XRD patterns (Figure 6b). Control experiments were carried out by attempting to introduce acridine red into porous crystals of **1**, the pore opening (with a diameter of 4.5 Å) of which does not allow the movement of acridine red into the body of

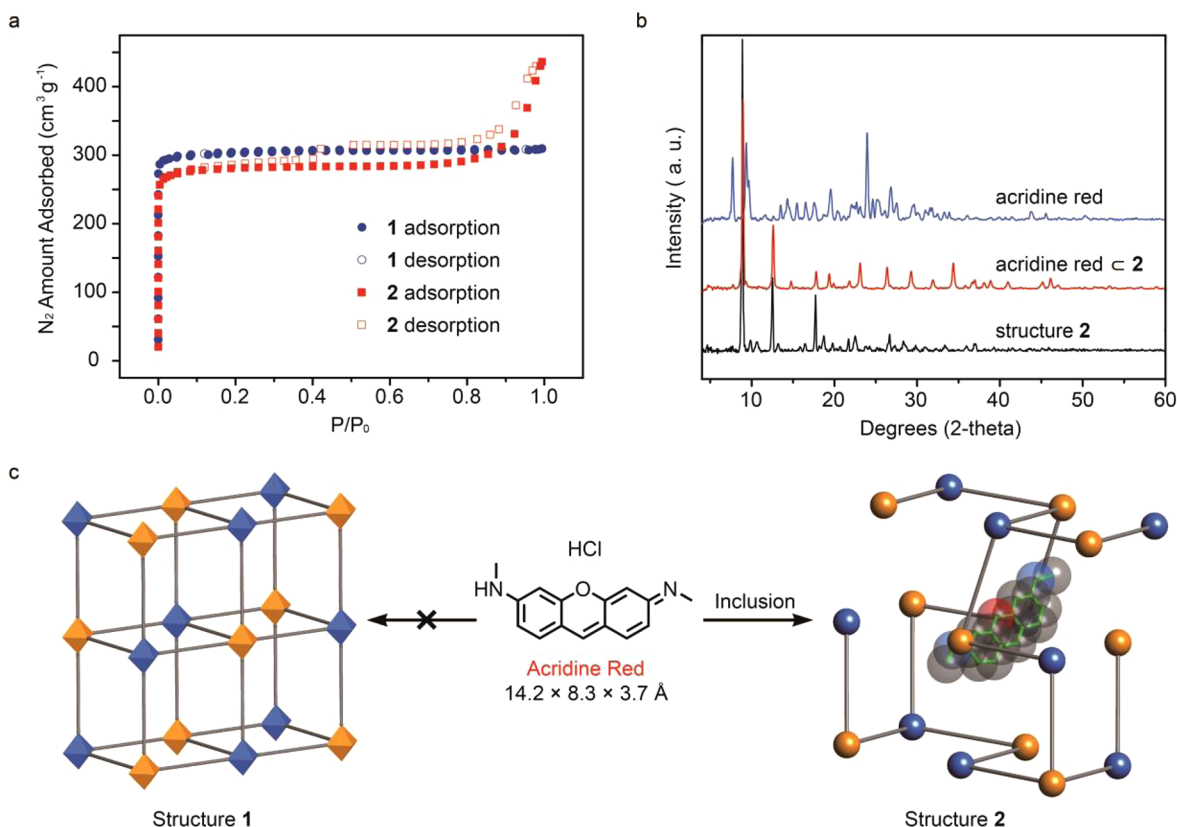


Figure 6. (a) Low-pressure N₂ adsorption isotherms of **1** and **2** at 77 K. (b) Powder XRD profiles for **2**, **2** after acridine red inclusion, and acridine red solid. (c) The pore opening of structure **2** allows the free movement of acridine red within the body of crystals, while our studies find no acridine red molecule in the channels of structure **1** due to size limit.

crystals. In the event, we established that no acridine red was found in the pores (Figure 6c and Figure S21 in the Supporting Information).

CONCLUSION

This study illustrates how ordered vacancies can be produced in a MOF using single-crystal to single-crystal transformation with full retention of cell dimensions and architectural stability. Furthermore, reactions on the vacancy sites maintain the crystallinity and yield MOFs whose structures could not be made in any other way. In essence, the elimination and addition reactions performed on macroscopic crystals of **1** and **2** make these extended structures objects similar to molecules in the precision with which they can be transformed. Thus, the study is an example of using crystals as molecules.

ASSOCIATED CONTENT

Supporting Information

Synthetic and characterization procedures; powder XRD of MOFs; low-pressure N₂ isotherms of MOFs; linker ratio determination by ¹H NMR; thermal gravimetric analysis; and X-ray crystallographic files (CIF) for **1**, **2**, **3-Li**, **3-Co**, **3-Cd**, **3-La**, **4-CH₃**, **4-NH₂**, **5-CH₃**, and **5-NH₂**. CCDC: 1007784–1007793. This material is available free of charge via the Internet at <http://pubs.acs.org>.

AUTHOR INFORMATION

Corresponding Author

qwli@fudan.edu.cn

Notes

The authors declare no competing financial interest.

ACKNOWLEDGMENTS

This work was supported by the National Natural Science Foundation of China (21101030), Creative Research Group of MOE (IRT1117), and Innovation Program of Shanghai Municipal Education Commission (14ZZ005).

REFERENCES

- (1) Tilley, R. J. D. *Defects in solids*; John Wiley & Sons, Inc.: NJ, 2008.
- (2) Baerlocher, C.; Xie, D.; McCusker, L. B.; Hwang, S.-J.; Chan, I. Y.; Ong, K.; Burton, A. W.; Zones, S. I. *Nat. Mater.* **2008**, *7*, 631–635.
- (3) Bernard, J. E.; Zunger, A. *Phys. Rev. B* **1988**, *37*, 6835–6856.
- (4) Özdas, E.; Kortan, A. R.; Kopylov, N.; Ramirez, A. P.; Siegrist, T.; Rabe, K. M.; Bair, H. E.; Schuppler, S.; Citrin, P. H. *Nature* **1995**, *375*, 126–129.
- (5) Chen, Z.; Cvelbar, U.; Mozetič, M.; He, J.; Sunkara, M. K. *Chem. Mater.* **2008**, *20*, 3224–3228.
- (6) Ramezani-pour, F.; Greedan, J. E.; Cranswick, L. M. D.; Garlea, V. O.; Donaberg, R. L.; Siewenie, J. *J. Am. Chem. Soc.* **2012**, *134*, 3215–3227.
- (7) Chezeau, J. M.; Delmotte, L.; Guth, J. L. *Zeolites* **1991**, *11*, 598–606.
- (8) Lee, K.-T.; Aswath, P. B. *Mater. Sci. Eng., A* **2003**, *352*, 1–7.
- (9) Dixona, E.; Hadermann, J.; Hayward, M. A. *J. Solid State Chem.* **2011**, *184*, 1791–1799.
- (10) Yaghi, O. M.; O’Keeffe, M.; Ockwig, N. W.; Chae, H. K.; Eddaoudi, M.; Kim, J. *Nature* **2003**, *423*, 705–714.
- (11) Kitagawa, S.; Kitaura, R.; Noro, S. *Angew. Chem., Int. Ed.* **2004**, *43*, 2334–2375.
- (12) Férey, G. *Chem. Soc. Rev.* **2008**, *37*, 191–214.

- (13) Furukawa, H.; Cordova, K. E.; O'Keeffe, M.; Yaghi, O. M. *Science* **2013**, *341*, 1230444.
- (14) Zhou, H.-C.; Long, J. R.; Yaghi, O. M. *Chem. Rev.* **2012**, *112*, 673–674.
- (15) Fang, Z.; Dürholt, J. P.; Kauer, M.; Zhang, W.; Lochenie, C.; Jee, B.; Albada, B.; Metzler-Nolte, N.; Pöppel, A.; Weber, B.; Muhler, M.; Wang, Y.; Schmid, R.; Fischer, R. A. *J. Am. Chem. Soc.* **2014**, *136*, 9627–9636.
- (16) Kozachuk, O.; Luz, I.; Xamena, I. L.; Noei, H.; Kauer, M.; Albada, H. B.; Bloch, E. D.; Marler, B.; Wang, Y.; Muhler, M.; Fischer, R. A. *Angew. Chem., Int. Ed.* **2014**, *53*, 7058–7062.
- (17) Feng, D.; Chung, W.-C.; Wei, Z.; Gu, Z.-Y.; Jiang, H.-L.; Chen, Y.-P.; Darenbourg, D. J.; Zhou, H.-C. *J. Am. Chem. Soc.* **2013**, *135*, 17105–17110.
- (18) Barin, G.; Krungleviciute, V.; Gutov, O.; Hupp, J. T.; Yildirim, T.; Farha, O. K. *Inorg. Chem.* **2014**, *53*, 6914–6919.
- (19) Vermoortele, F.; Ameloot, R.; Alaerts, L.; Matthessen, R.; Carlier, B.; Fernandez, E. V. R.; Gascon, J.; Kapteijn, F.; De Vos, D. E. *J. Mater. Chem.* **2012**, *22*, 10313–10321.
- (20) Eddaoudi, M.; Moler, D. B.; Li, H.; Chen, B.; Reineke, T. M.; O'Keeffe, M.; Yaghi, O. M. *Acc. Chem. Res.* **2001**, *34*, 319–330.
- (21) Space group $F23$ was chosen for structure **1** since the structure contains two types of SBUs (Zn_4ON_{12} and $Zn_4O(COO)_6$). If only one type of SBU with mixing N and O atoms exists in the framework, as shown with higher space group, it is not possible to obtain structure **2** after the single-crystal to single-crystal transformation, where two sets of new SBUs (one with O and the other one with N) arrange alternatively along the framework. The linker in structure **2** is not orientationally disordered, and there is no possibility of filling orientationally disordered linkers into the linker vacancies in **2**; thus, $F23$ was chosen for structures **4** and **5**. Several crystal structures show relatively high R values since these crystals have undergone two steps of single-crystal to single-crystal transformations, with multiple solvent exchange procedures. The high R values also reflect the disorder nature (solvents, ions, multilinks, and metals) of these crystals. See Supporting Information for more details.
- (22) Li, H.; Eddaoudi, M.; O'Keeffe, M.; Yaghi, O. M. *Nature* **1999**, *402*, 276–279.
- (23) Tranchemontagne, D. J.; Park, K. S.; Furukawa, H.; Eckert, J.; Knobler, C. B.; Yaghi, O. M. *J. Phys. Chem. C* **2012**, *116*, 13143–13151.
- (24) Bonneau, C.; Delgado-Friedrichs, O.; O'Keeffe, M.; Yaghi, O. M. *Acta Crystallogr.* **2004**, *A60*, 517–520.
- (25) Cohen, S. M. *Chem. Rev.* **2012**, *112*, 970–1000.
- (26) Lalonde, M.; Bury, W.; Karagiari, O.; Brown, Z.; Hupp, J. T.; Farha, O. K. *J. Mater. Chem. A* **2013**, *1*, 5453–5468.
- (27) Brozek, C. K.; Dincă, M. *Chem. Soc. Rev.* **2014**, *43*, 5456–5467.
- (28) Brozek, C. K.; Dincă, M. *J. Am. Chem. Soc.* **2013**, *135*, 12886–12891.
- (29) Bae, Y.-S.; Farha, O. K.; Hupp, J. T.; Snurr, R. Q. *J. Mater. Chem.* **2009**, *19*, 2131–2134.
- (30) Wang, Z.; Cohen, S. M. *J. Am. Chem. Soc.* **2007**, *129*, 12368–12369.
- (31) Kim, M.; Cahill, J. F.; Fei, H.; Prather, K. A.; Cohen, S. M. *J. Am. Chem. Soc.* **2012**, *134*, 18082–18088.
- (32) Botas, J. A.; Calleja, G.; Sanchez-Sanchez, M.; Orcajo, M. G. *Langmuir* **2010**, *26*, 5300–5303.
- (33) Song, X.; Kim, T. K.; Kim, H.; Kim, D.; Jeong, S.; Moon, H. R.; Lah, M. S. *Chem. Mater.* **2012**, *24*, 3065–3073.
- (34) Zhang, Z.; Zhang, L.; Wojtas, L.; Nugent, P.; Eddaoudi, M.; Zaworotko, M. J. *J. Am. Chem. Soc.* **2012**, *134*, 924–927.
- (35) Prasad, T. K.; Hong, D. H.; Suh, M. P. *Chem.—Eur. J.* **2010**, *16*, 14043–14050.
- (36) Zhao, J.; Mi, L.; Hu, J.; Hou, H.; Fan, Y. *J. Am. Chem. Soc.* **2008**, *130*, 15222–15223.
- (37) Manna, K.; Zhang, T.; Lin, W. *J. Am. Chem. Soc.* **2014**, *136*, 6566–6569.
- (38) Jacobs, T.; Clowes, R.; Cooper, A. I.; Hardie, M. J. *Angew. Chem., Int. Ed.* **2012**, *51*, S192–S195.
- (39) Wang, X.-J.; Li, P.-Z.; Liu, L.; Zhang, Q.; Borah, P.; Wong, J. D.; Chan, X. X.; Rakesh, G.; Li, Y.; Zhao, Y. *Chem. Commun.* **2012**, *48*, 10286–10288.
- (40) Fei, H.; Cahill, J. F.; Prather, K. A.; Cohen, S. M. *Inorg. Chem.* **2013**, *52*, 4011–4016.
- (41) Liu, T.-F.; Zou, L.; Feng, D.; Chen, Y.-P.; Fordham, S.; Wang, X.; Liu, Y.; Zhou, H.-C. *J. Am. Chem. Soc.* **2014**, *136*, 7813–7816.
- (42) Li, T.; Kozłowski, M. T.; Doud, E. A.; Blakely, M. N.; Rosi, N. L. *J. Am. Chem. Soc.* **2013**, *135*, 11688–11691.
- (43) Burrows, A. D.; Frost, C. G.; Mahon, M. F.; Richardson, C. *Angew. Chem., Int. Ed.* **2008**, *47*, 8482–8486.
- (44) Jiang, H.-L.; Feng, D.; Liu, T.-F.; Li, J.-R.; Zhou, H.-C. *J. Am. Chem. Soc.* **2012**, *134*, 14690–14693.
- (45) Deria, P.; Mondloch, J. E.; Tylianakis, E.; Ghosh, P.; Bury, W.; Snurr, R. Q.; Hupp, J. T.; Farha, O. K. *J. Am. Chem. Soc.* **2013**, *135*, 16801–16804.
- (46) Zhang, Z.; Gao, W.-Y.; Wojtas, L.; Ma, S.; Eddaoudi, M.; Zaworotko, M. J. *Angew. Chem., Int. Ed.* **2012**, *51*, 9330–9334.
- (47) Chen, Z.; Xiang, S.; Zhao, D.; Chen, B. *Cryst. Growth Des.* **2009**, *9*, 5293–5296.
- (48) Deng, H.; Doonan, C. J.; Furukawa, H.; Ferreira, R. B.; Towne, J.; Knobler, C. B.; Wang, B.; Yaghi, O. M. *Science* **2010**, *327*, 846–850.
- (49) Foo, M. L.; Matsuda, R.; Kitagawa, S. *Chem. Mater.* **2014**, *26*, 310–322.
- (50) Chevreau, H.; Devic, T.; Salles, F.; Maurin, G.; Stock, N.; Serre, C. *Angew. Chem., Int. Ed.* **2013**, *52*, S056–S060.
- (51) Katzenmeyer, A. M.; Canivet, J.; Holland, G.; Farrusseng, D.; Centrone, A. *Angew. Chem., Int. Ed.* **2014**, *53*, 2852–2856.
- (52) Kleist, W.; Jutz, F.; Maciejewski, M.; Baiker, A. *Eur. J. Inorg. Chem.* **2009**, *24*, 3552–3561.
- (53) Koh, K.; Wong-Foy, A. G.; Matzger, A. J. *Chem. Commun.* **2009**, *41*, 6162–6164.
- (54) Wang, L. J.; Deng, H.; Furukawa, H.; Gándara, F.; Cordova, K. E.; Peri, D.; Yaghi, O. M. *Inorg. Chem.* **2014**, *53*, 5881–5883.
- (55) Zhao, X.; Wu, T.; Bu, X.; Feng, P. *Dalton Trans.* **2011**, *40*, 8072–8074.
- (56) Zeng, M.-H.; Wang, B.; Wang, X.-Y.; Zhang, W.-X.; Chen, X.-M.; Gao, S. *Inorg. Chem.* **2006**, *45*, 7069–7076.
- (57) Cui, Y.; Xu, H.; Yue, Y.; Guo, Z.; Yu, J.; Chen, Z.; Gao, J.; Yang, Y.; Qian, G.; Chen, B. *J. Am. Chem. Soc.* **2012**, *134*, 3979–3982.
- (58) Xiao, D. J.; Bloch, E. D.; Mason, J. A.; Queen, W. L.; Hudson, M. R.; Planas, N.; Borycz, J.; Dzubak, A. L.; Verma, P.; Lee, K.; Bonino, F.; Crocella, V.; Yano, J.; Bordiga, S.; Truhlar, D. G.; Gagliardi, L.; Brown, C. M.; Long, J. R. *Nat. Chem.* **2014**, *6*, 590–595.
- (59) Morris, W.; Doonan, C. J.; Furukawa, H.; Banerjee, R.; Yaghi, O. M. *J. Am. Chem. Soc.* **2008**, *130*, 12626–12627.
- (60) Montoro, C.; Linares, F.; Procopio, E. Q.; Senkowska, I.; Kaskel, S.; Galli, S.; Masciocchi, N.; Barea, E.; Navarro, J. A. R. *J. Am. Chem. Soc.* **2011**, *133*, 11888–11891.
- (61) Doonan, C. J.; Morris, W.; Furukawa, H.; Yaghi, O. M. *J. Am. Chem. Soc.* **2009**, *131*, 9492–9493.
- (62) Vishnyakov, A.; Ravikovitch, P. I.; Neimark, A. V.; Bulow, M.; Wang, Q. M. *Nano Lett.* **2003**, *3*, 713–718.